A method for designing the longitudinal spacing of slope-stabilising shafts

Raffaele Di Laora & Vincenzo Fioravante

Acta Geotechnica

ISSN 1861-1125

Acta Geotech.
DOI 10.1007/s11440-017-0617-2

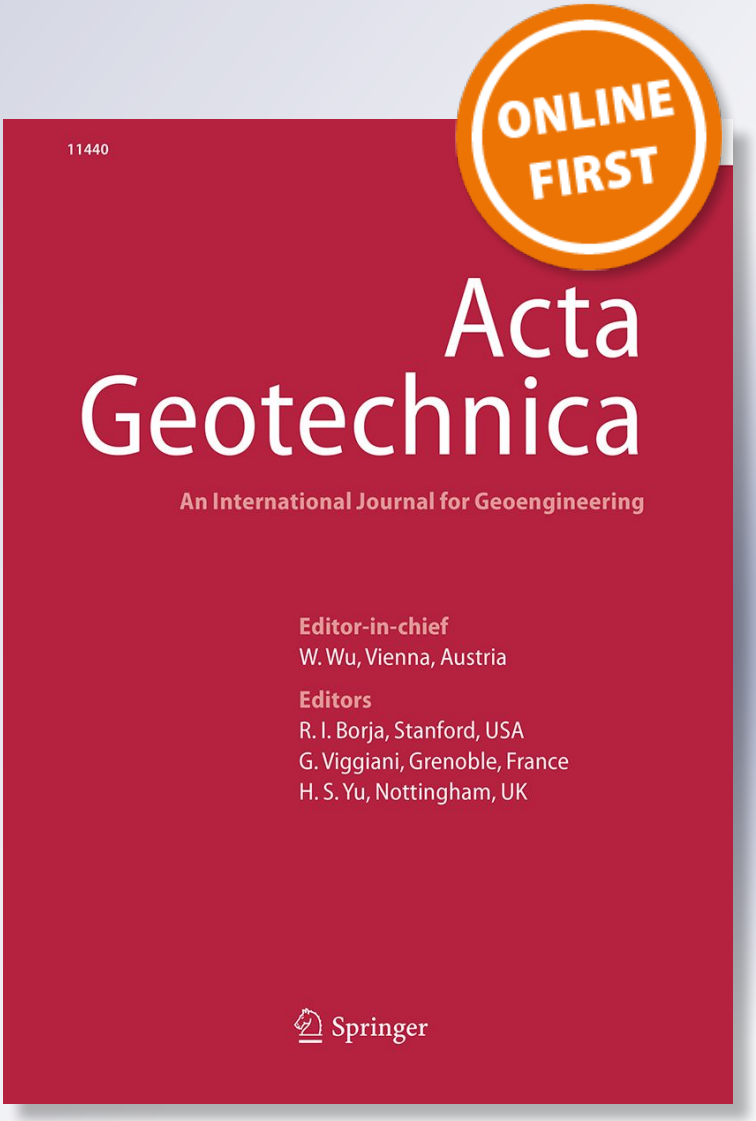

Springer

Your article is protected by copyright and all rights are held exclusively by Springer-Verlag GmbH Germany, part of Springer Nature. This e-offprint is for personal use only and shall not be self-archived in electronic repositories. If you wish to self-archive your article, please use the accepted manuscript version for posting on your own website. You may further deposit the accepted manuscript version in any repository, provided it is only made publicly available 12 months after official publication or later and provided acknowledgement is given to the original source of publication and a link is inserted to the published article on Springer's website. The link must be accompanied by the following text: "The final publication is available at link.springer.com”.

Author's personal copy

Acta Geotechnica
https://doi.org/10.1007/s11440-017-0617-2

RESEARCH PAPER

A method for designing the longitudinal spacing of slope-stabilising shafts

Raffaele Di Laora[1] · Vincenzo Fioravante[2]

Received: 24 February 2017 / Accepted: 9 December 2017
© Springer-Verlag GmbH Germany, part of Springer Nature 2018

Abstract
The work at hand deals with the design of the longitudinal spacing among rows of closely spaced large-diameter shafts used to stabilise a precarious slope. The problem under consideration is idealised through a conceptual framework where an unstable mass of an infinitely long slope pushes a stable portion of soil adjacent to shafts, leading to failure along a slip surface passing through the upper end of the reinforcement elements. By exploiting the upper bound theorem of plastic collapse, a closed-form solution is derived for the load required for the failure of the stable mass as a function of geometrical and mechanical parameters of the slope and the soil. Results are validated through physical model tests by means of geotechnical centrifuge. Given the satisfactory agreement between analytical and experimental results, the model is extended to evaluate the safety conditions of the reinforced slope.

Keywords Centrifuge test · Design · Limit analysis · Piles · Shafts · Slope stabilisation

1 Introduction

The use of piles or large-diameter shafts is a quite widespread engineering solution for the stabilisation of a shallow slow-moving landslide. The design of a row of piles involves the assessment of soil thrust on reinforcement elements and pile spacing. When multiple rows of piles or shafts are necessary due to a large extension of the unstable soil mass in the direction of the slope, the longitudinal spacing among rows of piles is a further parameter to be determined. The transversal and longitudinal spacing affect the critical failure mechanism which, in turn, has a crucial influence on the development of soil pressures on shafts and thereby the safety conditions of the reinforced slope. To facilitate understanding the above concepts, three different failure paths are depicted in Fig. 1. For each of them, body forces associated to soil weight would lead to failure if not contrasted by (1) the stresses developing along the specific slip surface and (2) the reinforcement–soil contact pressures. Path 1 involves pressures along the whole length of pile embedded in the unstable layer; path 2 exploits only partially such pressures while in path 3, not intersecting the shafts, soil cannot rely on any direct favourable contribution of the reinforcement. From path 1 to path 3, there is thereby a decreasing stabilising contribution of shaft–soil interaction pressures, yet the soil alone is more stable along the path 3 rather than paths 2 and 1, due to the geometry of the associated slip surface.

In the absence of reinforcement, the slope fails along the slip line n. 1 parallel to the slope surface, the other two paths being associated with larger safety. If a row of largely spaced piles or shafts is inserted in the unstable soil till penetrating for a sufficient depth the firm layer, soil may find path 2 as the easiest way to fail. If the spacing among the shaft decreases, the potential contribution of the reinforcement increases, so that there is a critical spacing below which the failure mechanism associated with the lowest level of safety corresponds to the path 3. In this case, the reinforcement, although does not contribute with interaction pressures, forces soil to fail according to a slip

✉ Raffaele Di Laora
raffaele.dilaora@unicampania.it

Vincenzo Fioravante
vincenzo.fioravante@unife.it

[1] Department of Civil Engineering, Design, Building and Environment, Università della Campania "Luigi Vanvitelli", Aversa, CE, Italy

[2] Department of Engineering, University of Ferrara, Ferrara, Italy

Published online: 04 January 2018

Author's personal copy

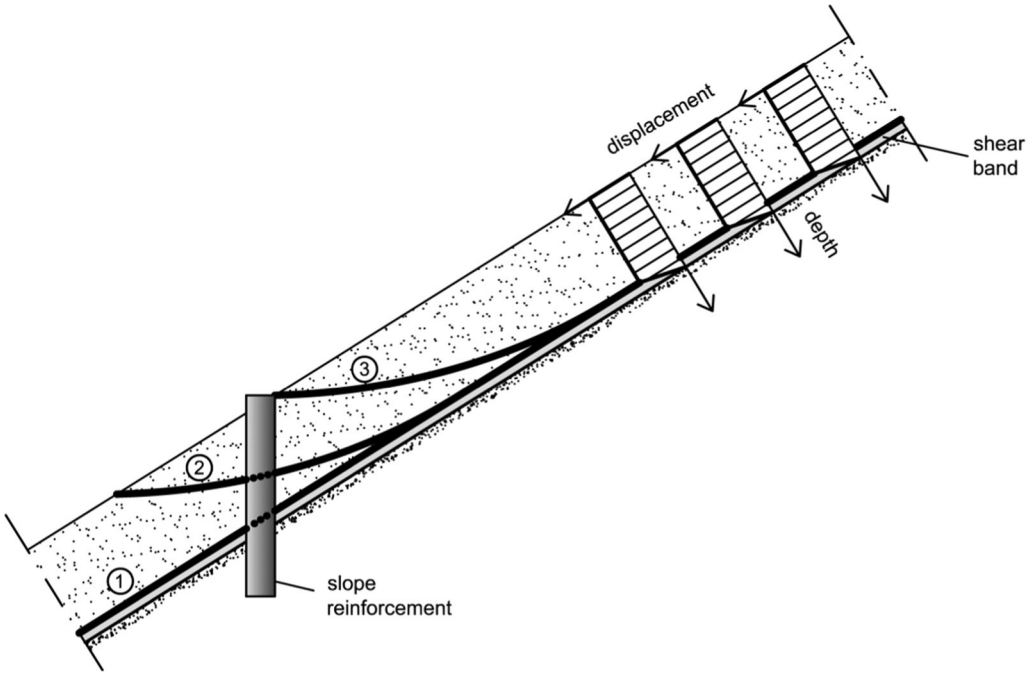

Fig. 1 Problem under consideration

surface associated with larger safety compared to the unreinforced slope.

The evaluation of the pressures that isolated or rows of piles may offer in favour of stability was studied, among others, by Ito and Matsui [15], De Beer and Carpentier [8] and Viggiani [24]. The first two contributions dealt with the evaluation of the ultimate load of a row of piles. A discussion on the applicability of these methods can be found in Bosscher and Gray [5]. Viggiani [24] provided analytical solutions for a single free-head pile embedded in fine-grained soil, considering undrained conditions and performing a total stress analysis in the framework of limit equilibrium method. With a similar approach, Muraro et al. [20] obtained the solution for the case of a rigid (not yielding) single free-head pile in drained conditions. A number of contributions dealt with pile–soil interaction [3, 12, 14, 22], and other investigators focused on general aspects of design by performing numerical analyses (e.g. [13, 16, 17, 21]), while fewer research exploited physical models to explore the behaviour of reinforced slopes of finite length (e.g. the recent centrifuge experiments performed by Zhang et al. [25, 26]).

Despite numerous studies, there are still many uncertainties and issues on the topic. A general lack in previous studies is that the methods proposed in the literature refer to the critical surface corresponding to the unreinforced slope, and this, as the discussion above suggests, may lead to a large overestimation of the stability conditions of a slope reinforced with closely spaced shafts given that soil finds an easier way to fail, without intersecting the reinforcement. In addition to this, to stabilise a slope with a predominant longitudinal dimension, several rows of piles or shafts placed at a certain distance from each other have to be adopted, yet no explicit method exists for the design of such spacing.

To furnish a contribution on this aspect, in this work the mechanism n. 3 described above is studied analytically to evaluate the safety conditions associated with a specific longitudinal dimension of the unstable soil mass, under the hypothesis of plane strain conditions (i.e. strains perpendicular to the direction of sliding are zero).

2 Proposed problem decomposition

The problem at hand consists of a slope of inclination α which, due to phenomena like progressive failure, possesses a reduced value δ of shearing resistance angle at soil–bedrock interface for a length L_u and is therefore stabilised through the insertion of closely spaced shafts, so that soil does not flow among them. A schematic sketch of the problem is reported in Fig. 2 where the slip surface follows the above-described path 3. It is convenient to refer to a conceptual framework where the problem geometry is decomposed in two distinct zones, specifically a thrust zone of length L_t which slides, for $\delta < \alpha$, along the direction of the slope thereby forcing the remaining part of soil of length ξ_s $(= L_u - L_t)$ to fail according to a rotational mechanism along a curved surface passing through the upper end of the reinforcement. This decomposition,

Author's personal copy

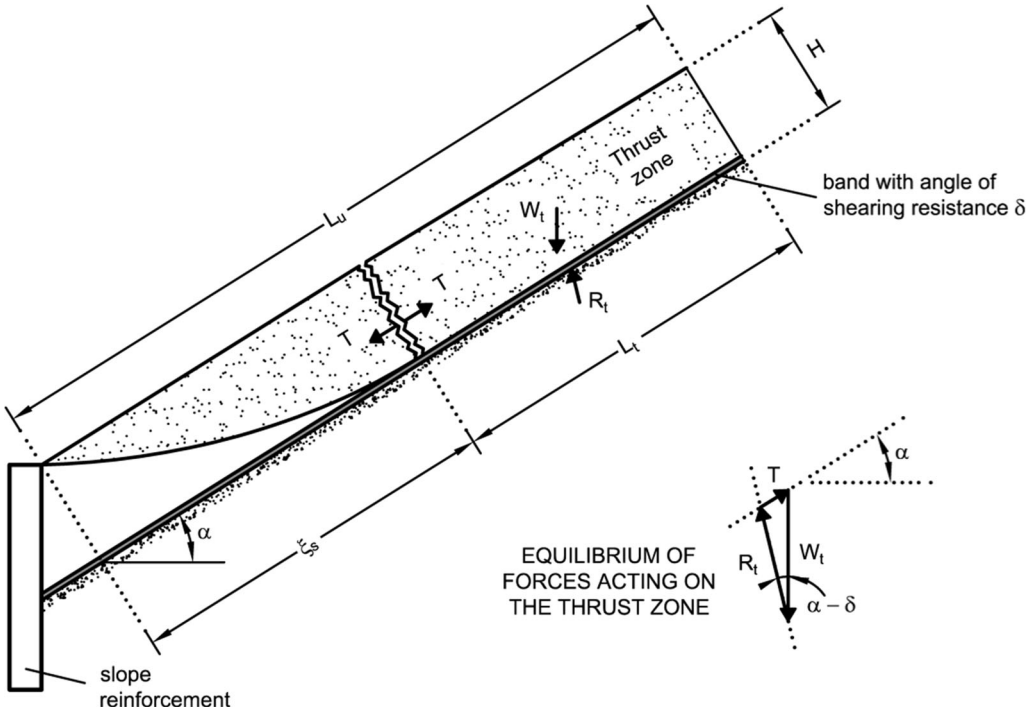

Fig. 2 Conceptual framework for the sliding mechanism of a slope stabilised by closely spaced shafts

although not rigorous because the combination of a translational and a rotational mechanism is kinematically inadmissible, offers the following advantages: (1) it allows results to be expressed in closed form; (2) permits a direct validation of results through laboratory experiments where the slope failure is achieved through the application of a load; (3) permits to quantify the safety conditions through the ratio of failure load and unstabilising action. Accordingly, an upper bound to the failure load of the resistant zone will be sought. To facilitate understanding, the main theoretical aspects associated with the limit analysis technique utilised in this work are briefly recalled in the following.

3 Upper-bound solution for failure load

When tackling collapse problems, it is very common the use of limit analysis. Instead of seeking an exact value of failure load, upper and lower bounds which bracket the true value can be found by this technique. Ignoring whether the equilibrium or the compatibility condition, theorems of plastic collapse will furnish rigorous upper and lower bound values, respectively, to the failure load if an associative flow rule is considered for the soil material.

The upper bound theorem states that for any arbitrary compatible failure surface (i.e. no gaps or overlaps exist within the body) such that the work done by external loads and body forces equals the energy dissipated along the failure surface, the external loads represent an upper bound to the true collapse loads. This theorem reflects the fact that soil may find a different failure surface associated with lower external loads. (Details on the application of theorems of plastic collapse to geotechnical problems may be found in many textbooks, e.g. [7] and [1].)

From a practical standpoint, the application of the upper bound theorem is herein carried out by means of the following steps:

1. A compatible rotational failure mechanism is assumed, the geometry of which is function of different variables;
2. The work done by self-weight and external loads due to the displacement (or velocity) field assumed for the mechanism is computed;
3. The internal dissipation of energy by plastically deformed regions associated with the mechanism is evaluated;
4. The external load is derived through the work equation (i.e. by equating the quantities derived at steps 2 and 3);
5. By varying the values of the independent variables as defined in step 1, the mechanism layout that leads to the least external loads is detected.

With reference to step 1, an important consequence of the associative flow rule is that in a rotational mechanism for drained conditions is that velocity (or displacement) vector and failure surface make always an angle φ (Fig. 3).

Author's personal copy

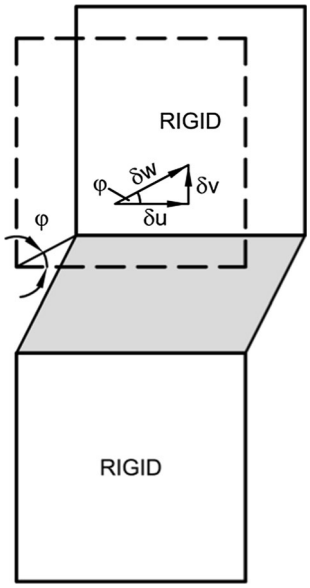

Fig. 3 Slip surface and displacement (or velocity) field for $\varphi > 0$

Therefore, a compatible failure surface can be only a logarithmic spiral of equation:

$$r(\theta) = r_0\, e^{(\theta-\theta_0)\tan\varphi} \tag{1}$$

with r the radius at any angle θ and r_0 the initial radius (i.e. for $\theta = \theta_0$). Such a curve degenerates in a straight line for $r_0 \to \infty$.

An arc of logarithmic spiral necessitates of three parameters to be fully described, e.g. initial radius r_0 and initial and final angle with the horizontal axis θ_0 and θ_s, and therefore, the solution of the problem at hand should be identified as the particular combination of the three values of the parameters above which gives rise to the least applied load q.

Nevertheless, with reference to the investigated problem, further considerations may simplify the tractation, as shown in Fig. 4. The sliding surface must pass by point B and must be tangent, in the same point, to the base. By making use of these two conditions, given the associative flow rule of soil material the velocity in B must make an angle φ with the slope and therefore the centre of rotation must lie on a line passing through B and inclined of $(90° + \varphi)$ with respect to the slope direction. For any radius r_0, the angle θ_0 is immediately identified, whereas the final angle θ_s is determined by the intersection of the logarithmic spiral with soil surface (point C), having distance ξ_s from the applied load acting on the line AB. It follows that the problem has now 1 degree of freedom and any value of r_0 (or, alternatively, ξ_s or θ_s) corresponds to a specific value of the load q. The value of r_0, ξ_s or θ_s that leads to the lowest q determines the critical failure surface,

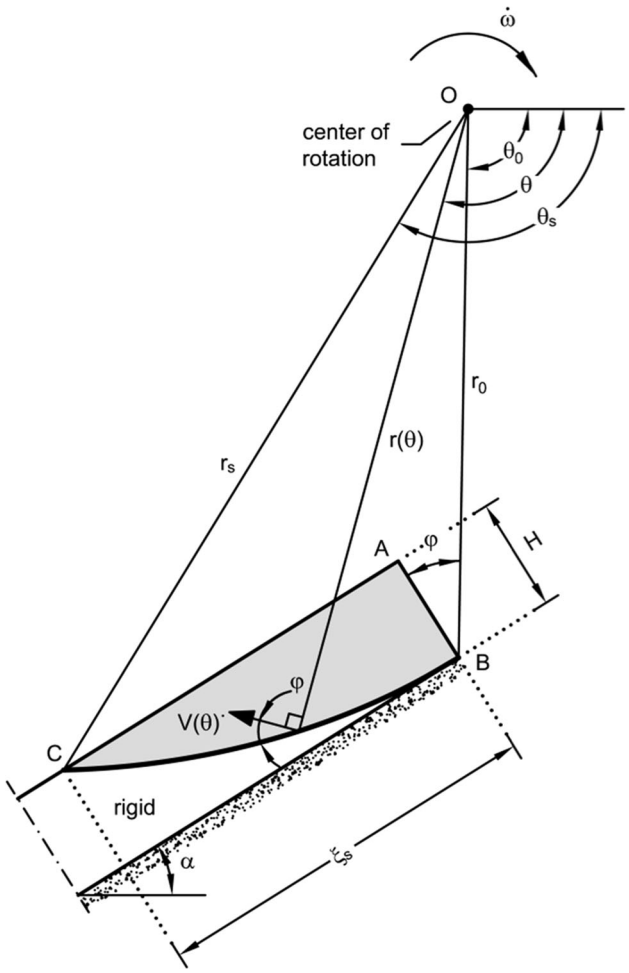

Fig. 4 Slip surface and velocity field for the problem under consideration

and the associated load is the sought upper bound to the failure load.

3.1 Geometry of the mechanism

It is rather straightforward to determine the geometry of any failure mechanism by simple trigonometric considerations. With reference to Fig. 4, initial angle θ_0 is function of the soil shearing resistance angle φ and the inclination of the slope α according to the equation:

$$\theta_0 = 90° + \varphi - \alpha \tag{2}$$

For any final angle θ_s, taken for convenience as the independent variable, the geometry of the slip surface is univocally determined, and intersects soil surface at an abscissa

$$\xi_s = H\tan\Delta_1 = H\tan(180° + \theta_0 - \theta_s - \varphi - \Delta_2) \tag{3}$$

Δ_1 and Δ_2 being the angles $A\widehat{B}C$ and $O\widehat{C}B$, respectively. Δ_2 can be computed through the equation:

Author's personal copy

$$\begin{aligned}\Delta_2 &= \mathrm{O}\widehat{\mathrm{C}}\mathrm{B} \\ &= \sin^{-1}\left[\sin(\theta_s-\theta_0)\cdot\left(1+e^{2(\theta_s-\theta_0)\tan\varphi}\right.\right. \\ &\quad \left.\left.-2e^{(\theta_s-\theta_0)\tan\varphi}\cos(\theta_s-\theta_0)\right)^{-\frac{1}{2}}\right]\end{aligned} \tag{4}$$

The initial radius is:

$$r_0 = H\frac{\sin\Delta_2}{\sin(\theta_s-\theta_0)\cos\Delta_1} = \xi_s\frac{\sin\Delta_2}{\sin(\theta_s-\theta_0)\sin\Delta_1} \tag{5}$$

3.2 Rate of work due to self-weight and external load

The rate of work due to self-weight of the portion of sliding soil rotating at clockwise angular velocity $\dot{\omega}$ according to the rotational mechanism in Fig. 4 may be computed by evaluating the work rates $\dot{W}_1$,$\dot{W}_2$ and $\dot{W}_3$ due to the soil weight in the regions OCB, OCA and OAB, respectively, then performing the algebraic summation $\dot{W}_1 - \dot{W}_2 - \dot{W}_3$. Other combinations of areas may be considered; however, this strategy is adopted here following other works dealing with upper-bound solutions for slope stability problems like Chen [7], Michalowski [18] and Ausilio et al. [2].

Figure 5 depicts the detailed computation of the three contributions above, which are found to be:

$$\begin{aligned}\dot{W}_1 &= \dot{\omega}\,\gamma\,\frac{(3\tan\varphi\cos\theta_s+\sin\theta_s)r_s^3-(3\tan\varphi\cos\theta_0+\sin\theta_0)r_0^3}{3(1+9\tan^2\varphi)} \\ \dot{W}_2 &= \dot{\omega}\,\gamma\left[-\frac{1}{6}Hr_0(H\sin\alpha-2r_0\cos\theta_0)\sin\varphi\right] \\ \dot{W}_3 &= \dot{\omega}\,\gamma\left[-\frac{1}{6}r_s\xi_s\left(\begin{matrix}2H\sin\alpha-2r_0\cos\theta_0\\ +\xi_s\cos\alpha\end{matrix}\right)\sin(\theta_s+\alpha)\right]\end{aligned} \tag{6}$$

with γ the unit weight of the soil and $r_s = r(\theta_s)$. Note that the rate of work due to self-weight is negative for the assumed rotational mechanism (i.e. soil weight represents a stabilising contribution).

From the same figure, it is simple to verify that the rate of work due to the external load is given by:

$$\dot{Q} = \dot{\omega}\,qH(r_0\cos\varphi - h) \tag{7}$$

where q is the average normal stress due to the applied load. Note that the rate of work due to the external load is positive (i.e. the load furnishes an instabilising contribution).

3.3 Dissipation of energy

The dissipation of energy D in the layer of plastic shearing (grey area in Fig. 3) may be written as:

$$D = \tau\cdot\delta u - \sigma\cdot\delta v = \delta u(\tau-\sigma\tan\varphi) = c\cdot\delta u \tag{8}$$

where σ and τ are the normal and shear stress (the former to be taken as positive in compression), whereas δu and δv are the components of the displacement along and perpendicular, respectively, to the slip surface. It is interesting to note that internal dissipation is related merely to the cohesion of the soil material. It follows that for a cohesionless soil there is no internal dissipation, and therefore, the soil can be considered at the same time both dissipative and conservative, which is self-contradicting. This seems to indicate that the flow rule for a frictional material cannot be associative [1]. The possibility of considering a non-associative material for seeking a better upper bound is explored in Drescher and Detournay [9]; however, these considerations are not employed in the present work.

The differential rate of dissipation along the logarithmic spiral slip line is found by multiplying the differential segment length ($r{\cdot}d\theta/\cos\varphi$) by the cohesion c times the component of velocity parallel to the discontinuity, $V{\cdot}\cos\varphi$. By integrating the differential rate of dissipation over the whole length of the log-spiral arc, one obtains the rate of dissipation as:

$$\dot{D} = \int_{\theta_0}^{\theta_s} c(V\cos\varphi)\frac{r\cdot d\theta}{\cos\varphi} = \dot{\omega}\frac{c}{2\tan\varphi}\left(r_s^2-r_0^2\right) \tag{9}$$

3.4 Derivation of the external load

The external load can be now computed through the work equation:

$$\dot{Q} + \dot{W}_1 - \dot{W}_2 - \dot{W}_3 = \dot{D} \tag{10}$$

from which one, after algebraic manipulation (see Appendix), can derive the collapse load, in the ensuing denoted by q_{lim}, as:

$$\begin{aligned}\frac{q_{\mathrm{lim}}}{\gamma H} = &\frac{\dfrac{r_0}{H}\sin\varphi\left(2\dfrac{r_0}{H}\cos\theta_0-\sin\alpha\right)}{-\dfrac{\xi_s}{H}\dfrac{r_s}{H}\left(\dfrac{\xi_s}{H}\cos\alpha+2\sin\alpha-2\dfrac{r_0}{H}\cos\theta_0\right)\sin(\theta_s+\alpha)} \\ &+\frac{2\left[\begin{matrix}(3\tan\varphi\cos\theta_0+\sin\theta_0)\left(\dfrac{r_0}{H}\right)^3\\ -(3\tan\varphi\cos\theta_s+\sin\theta_s)\left(\dfrac{r_s}{H}\right)^3\end{matrix}\right]}{1+9\tan^2\varphi} \\ &+3\frac{c}{\gamma H}\cot\varphi\left[\left(\frac{r_s}{H}\right)^2-\left(\frac{r_0}{H}\right)^2\right] \\ &\hline 6\left(\frac{r_0}{H}\cos\varphi-\frac{h}{H}\right)\end{aligned} \tag{11}$$

Author's personal copy

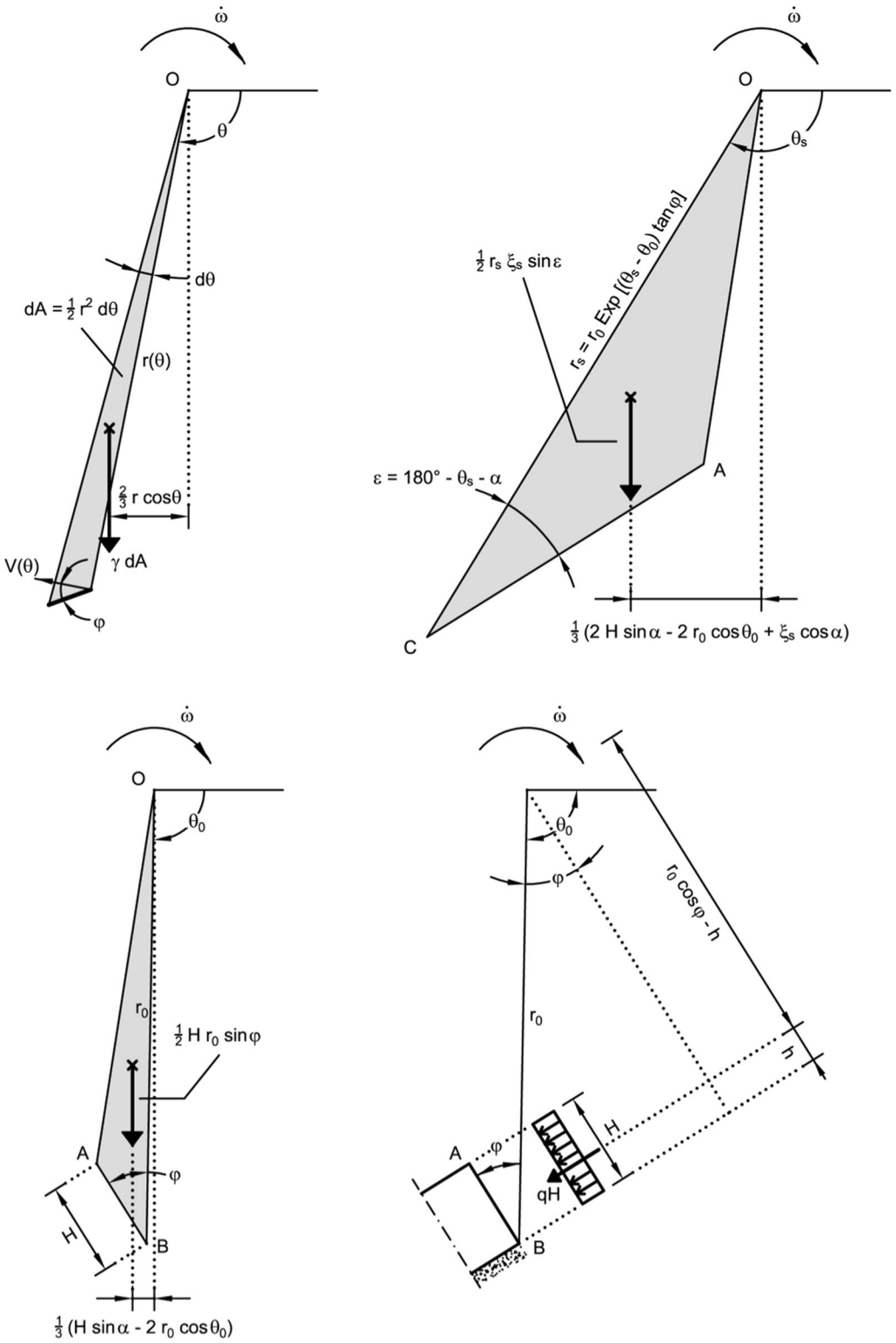

Fig. 5 Detailed calculation of the work done by self-weight and external load

Author's personal copy

Figure 6 depicts the failure load $q_{\lim}$, initial radius r_0 and angle covered by failure surface, $(\theta_s - \theta_0)$, as a function of the only independent variable ξ_s, for two hypotheses on the position of applied load ($h/H = 1/2$ and $h/H = 1/3$). By inspection of these diagrams, a number of aspects are noteworthy: (1) despite r_0 and $(\theta_s - \theta_0)$ formally depend on soil properties and load position (see Eqs. 2–5), the curves are not distinguishable (Fig. 6b); it follows that the geometry of the failure surface depends mainly on the geometry of the problem under consideration; (2) by increasing ξ_s, initial radius increases while the angle covered by the failure surface decreases, that is the failure surface becomes more "smooth", tending to a straight line; (3) failure load $q_{\lim}$ diminishes with ξ_s up to a certain value, because soil is facilitated to slip on a smoother surface, and then increases when this effect is counterbalanced by the increasing resistance along the wider surface; (4) the presence of cohesion in the soil has a remarkable role in increasing failure load; (5) a smaller value of h/H is detrimental for slope stability due to the increasing distance from the centre of the mechanism; (6) for increasing values of ξ_s the position of the instabilising force has no influence on the limit load; this indicates that the failure mechanism is tending to a translational one, as confirmed by the increasing value of radius r_0, and gives an idea of how small is the influence of the kinematic mismatch involved in the approximated combined mechanism proposed in this work.

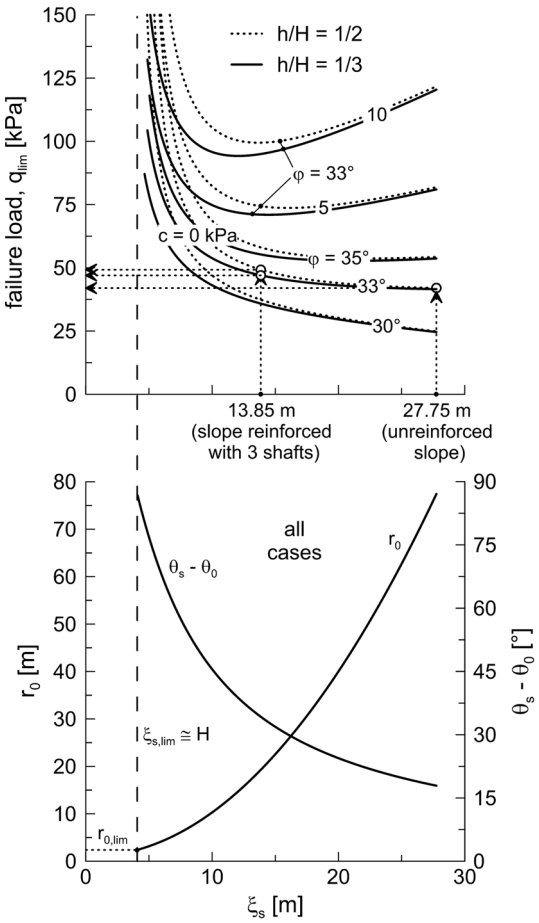

Fig. 6 Critical failure surfaces and associated values of external load for different values of c, φ and h/H

4 Centrifuge test modelling

The problem under consideration was tackled experimentally by means of the ISMGEO (Istituto Sperimentale Modelli Geotecnici, Seriate–BG–Italy) geotechnical centrifuge (IGC), made up of a symmetrical rotating arm with a diameter of 6 m, a height of 2 m and a width of 1 m. The arm holds two swinging platforms, one used to carry the model container and the other the counterweight; during the test, the platforms lock horizontally to the arm to prevent transmitting the working loads to the basket suspensions. An outer fairing covers the arm; the arm and the cover concurrently rotate to reduce air resistance and perturbation during flight; further details of the centrifuge can be found in Baldi et al. [4]. It is worth recalling that, in a physical model subjected to a centrifuge acceleration N times larger than the acceleration of gravity g, geometrical dimensions are N times smaller than the ones in the prototype, whereas both stresses and strains are scaled 1-to-1. A complete set of similarity relationships between physical model and prototype is available in many scientific contributions (e.g. [19, 23]). The adopted geometrical scaling factor of the models was $N = 50$, and therefore, the test was conducted under an acceleration field of 50 g, which was reached in the centre of gravity of the model mass.

The model and prototype geometrical dimensions are listed in Table 1. Three static tests were performed: the unreinforced sandy landslide and the landslide reinforced with 1 central and 3 aligned shafts. Figure 7 shows the general layout of the tests. (All measures refer to the model scale.) The rock slope was modelled through a lightweight concrete block fixed to the centrifuge strong box with shear wave velocity $V_S \approx 950$ m/s as deduced with reference to linear elasticity from the Young's modulus and Poisson's ratio measured in uniaxial cylindrical tests with local strain measurements. The sandy slope was modelled through a very fine and uniform silica powder, derived by grinding and sieving pit rocks, named FF sand (FFS), mainly consisting of sub-angular particles and made of 98.2% quartz, 1.3% feldspar and 0.5% mica. The main characteristics of FFS are:

- maximum and minimum dry density, $\gamma_{d,\max} = 14.78$ - kN/m^3, $\gamma_{d,\min} = 11.58$ kN/m^3,

Author's personal copy

Table 1 Geometrical dimensions at the model and the prototype scale

	Dimension	Model scale	Prototype scale
Sandy slope	Thickness, H	80 mm	4 m
	Length, L	555 mm	27.75 m
	Inclination, α	32°	32°
Shaft	External diameter, d	70 mm	3.5 m
	Height, H_s	200 mm	10 m
	Shaft spacing, s	105 mm	5.25 m

- maximum and minimum void ratio, $e_{max} = 1.211$, $e_{min} = 0.732$,
- specific density, $G_s = 2.61$,
- mean particle size, $D_{50} = 0.093$ mm,
- uniformity coefficient, UC = 1.88.

The critical state parameters are:

- shearing resistance angle at critical state, $\phi'_{cv} = 33°$,
- critical stress ratio, $M = 1.35$,
- void ratio at $p' = 1$ kPa, $e_\Gamma = 1.15$,
- slope of the critical state line in the e-ln(p') plane, $\lambda = 0.026$.

The sand layer was reconstituted by tamping the sand, with a moisture content of 5%, in four horizontal layers 20 mm thick, having inclined the box − 32° to the horizontal, so that the strata were parallel to the rock slope. The average relative density achieved at the end of the 50 g in–flight consolidation was $D_R \approx 40\%$, computed from the variation in the volume of the sand, as measured in few points by vertical and rotational potentiometer transducers. The knowledge of relative density can be therefore utilised to estimate a unit soil weight of 12.5 kN/m^3. The soil–concrete interface was rough and produced an interface friction angle δ' equal to φ'_{cv} (in the ensuing indicated with φ for brevity), as deduced from several interface direct shear tests. The model container was designed with rigid walls to confine the model in the transversal direction (Fig. 7). The side friction between the soil and the container walls was minimised by lubricating the lateral surfaces. Rock sockets were pre-formed, and the shafts inserted and grouted before tamping the sand around them. The reinforcing shafts were modelled by aluminium alloy cylinders of external diameter $d = 70$ mm. The selection of the cylinder thickness is aimed at obtaining a ratio between prototype and model flexural stiffness equal to N^4 [11, 19]. Referring to a prototype concrete shaft with Young's modulus equal to 35 GPa with an external diameter of 3.5 m and an internal diameter of about 2.6 m,

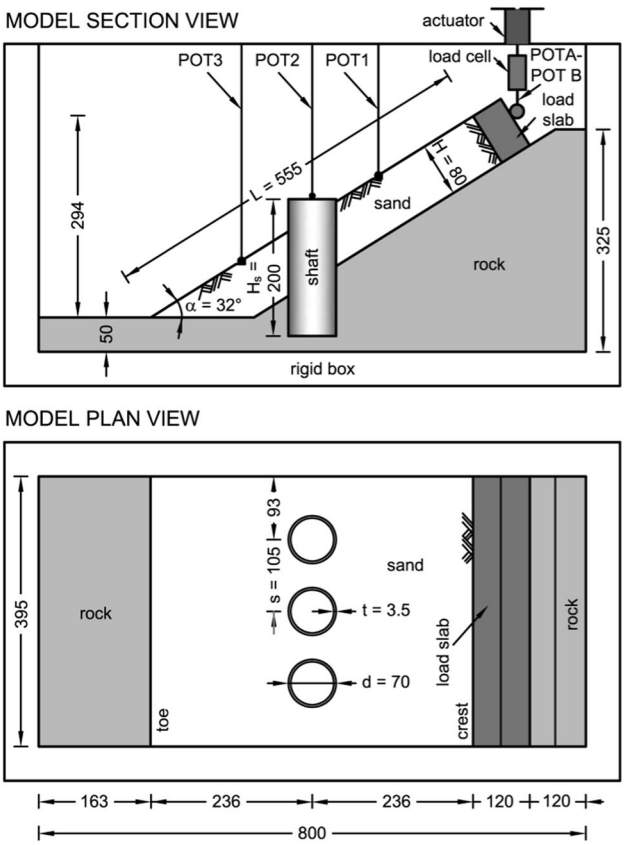

Fig. 7 Layout of the tests (model scale): section and plane views of the reinforced model. All dimensions are in mm

the prototype must possess a wall thickness of 3.5 mm. The centre-to-centre shaft spacing in the tests with 3 reinforcing piers was equal to 1.5 $d = 105$ mm. Each model was prepared at 1 g, and then it was embarked into the centrifuge, accelerated to 50 g and allowed to consolidate due to the self-weight, until settlements at surface reached a constant value. The landslide was triggered by a displacement-controlled piston which pushed down the top of the slope through a rigid slab connected to a hydraulic actuator. The raft was allowed to slide parallel to the slip interface to produce a uniform displacement field gradually increasing until failure.

Figure 8 shows the failure modes directly observed in the test with 1 and 3 shafts. It can be immediately recognised that in the case of an isolated reinforcing element soil flows around the shaft, which is thus intersected by the failure surface, that is according to the path 2 in Fig. 1. On the contrary, for the case of three shafts, soil fails just behind the reinforcement (path 3). The latter mechanism is investigated in the next section.

Author's personal copy

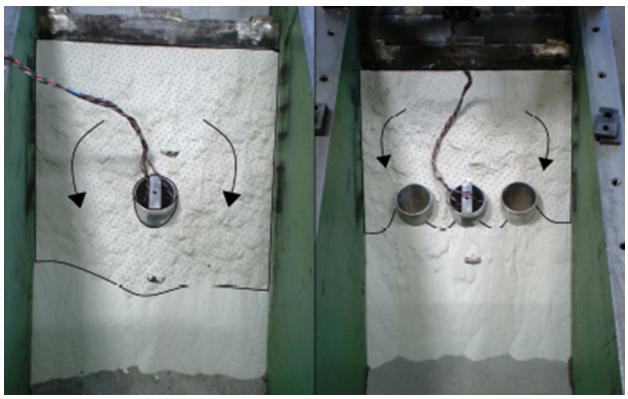

Fig. 8 Failure surfaces for the tests with 1 and 3 shafts

5 Validation of the proposed solution through centrifuge test results

5.1 Failure loads

The proposed model is applied to interpret the centrifuge tests described above. The first, straightforward application can be made with reference to the unreinforced slope. Given the soil strength parameters obtained from laboratory tests ($c = 0$, $\varphi = 33°$), Fig. 6 suggests that slope failure occurs for the highest possible value of ξ_s that, for the case under consideration, is the slope length (= 27.75 m at the prototype scale). The failure load furnished by the proposed method is 42 kPa for any position of the applied load. In the same fashion, the maximum load for the test with three shafts may be evaluated. Given the very small spacing among the shafts, no flow occurs within them and hence soil cannot but fail without intersecting slope reinforcement, so that ξ_s is equal to the distance ξ_p (= 13.85 m) between applied load and the shafts' axis. For $\xi_s = \xi_p$ Eq. (11) provides a failure load $q_{\lim}$ ranging between 47 and 49 kPa. As an additional step, for the case of the unreinforced soil, the failure load may be also used to estimate to whole load–displacement curves of the control points, as outlined below.

5.2 Load–displacement curves

It is apparent that a rigorous description of the load–displacement behaviour of any point in the soil mass requires complex analyses involving all the geometrical and mechanical parameters of the problem, including a realistic assumption for the constitutive law of the soil material. Instead, it is herein tried to outline a simple method to quickly estimate the load–displacement curve of any point for the case of unreinforced slope. The method, while taking into account–directly or indirectly—all the salient problem parameters, requires few quantities easy to determine. Specifically, it is proposed to describe the load–displacement curve (i.e. the relationship between the applied load q and the displacement s_ξ at any location ξ) through a hyperbolic law having equation:

$$s_\xi(\xi, q) = \frac{q}{K_0(\xi) \cdot \left[1 - \left(\frac{q}{q_{\lim}}\right)^{0.2}\right]} \tag{12}$$

Such an hyperbolic approach therefore requires the knowledge of only two parameters, i.e. the asymptote $q_{\lim}$, previously determined, and the initial stiffness K_0 at the location ξ. To estimate the latter, one may suppose that the displacement field is one-dimensional so that all points at the same coordinate ξ will experience the same displacement in the direction of the slope, and neglect shear stress at the base. Under these assumptions, the initial stiffness can be simply calculated as:

$$K_0(\xi) = \frac{E_0}{L - \xi} \tag{13}$$

where E_0 is the Young's modulus of the soil at small strain. For the case at hand, considering the low confinement pressure, both laboratory testing and the empirical relationship proposed by Fioravante [10] furnish a value of about 28 MPa.

5.3 Comparison with experimental data

Figure 9 depicts vertical displacements of points on soil surface against applied load for the unreinforced slope (Fig. 9a) and for the 3-shafts reinforcement (Fig. 9b). Also shown in the graph are the failure loads predicted by the analytical method via Eq. (11). Figure 9a also shows load–displacement curves predicted by Eq. (12). Vertical component of displacement is naturally found by multiplying the displacement along ξ by $\sin\alpha$. Considering the simplicity of the method and the amount of variables—and associated uncertainties—affecting the system response, the analytical results are in remarkable agreement with experimental data both for initial stiffness (pronounced in the graph owing to the log-scale in the horizontal axis) and the evolution of the displacements by approaching the failure load. The good performance of the model is confirmed for the reinforced slope in Fig. 9b, where measured displacements approach a vertical asymptote at $q = 46$ kPa, corresponding to an error between 2 and 6%, depending on the assumption on the position of the resultant thrust.

Author's personal copy

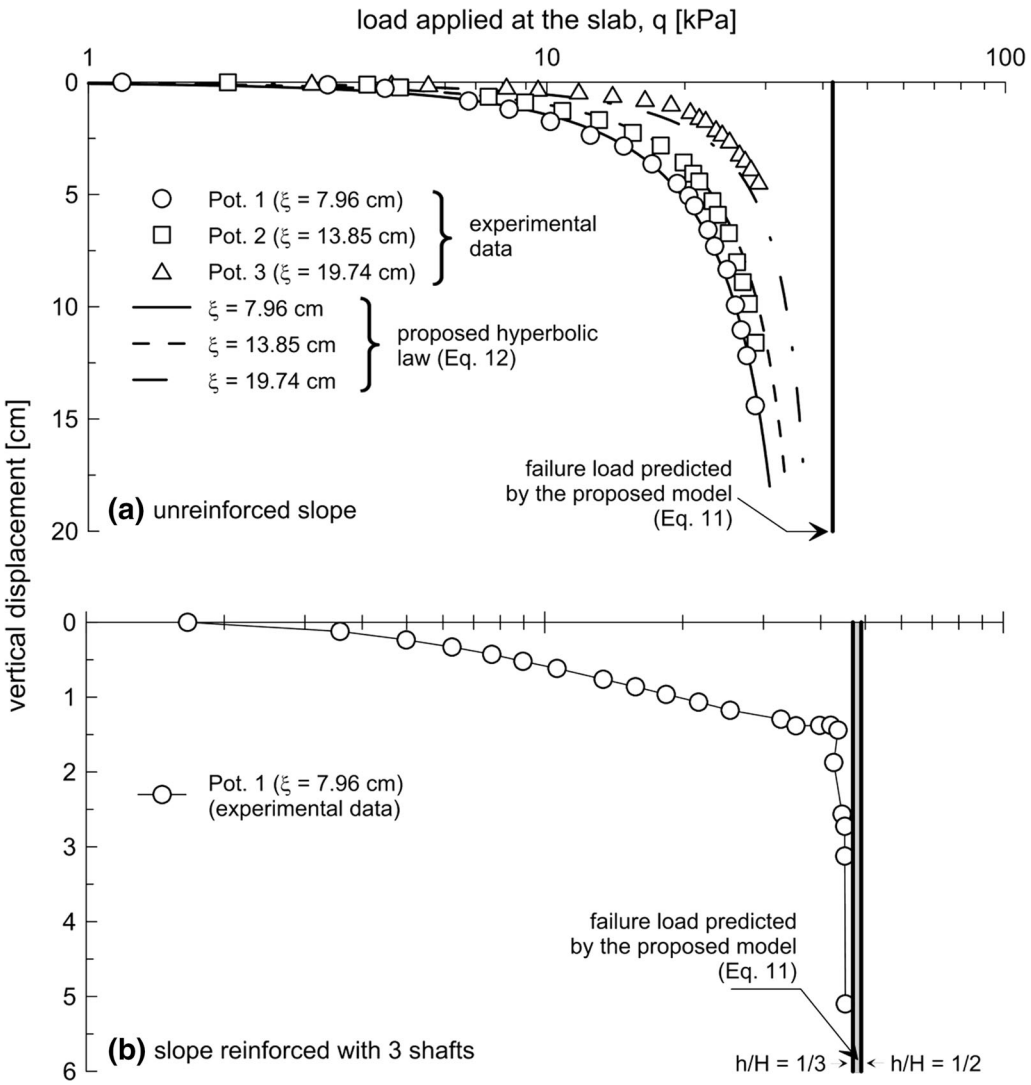

Fig. 9 Comparison between failure load and displacements predicted by the proposed methods and load–displacement curves measured in the tests for unreinforced slope (**a**) and slope reinforced with 3 shafts (**b**)

6 Factor of safety of the reinforced slope and design of longitudinal spacing

The above findings may directly be employed to interpret the centrifuge test results where the rigid slab, that pushes soil by applying a one-dimensional displacement field, represents the thrust zone L_t in Fig. 2 which displaces uniformly along the direction of the slope. As a step towards the definition of a design methodology, a measure of the safety conditions of the reinforced slope may be defined considering that the resistant zone of length ξ_s attains failure conditions for a load T_f given by Eq. (11) ($T_f = q_{\lim} H$), whereas the unstable soil applies a thrust T which can be easily derived from equilibrium considerations as:

$$T = \gamma H (L_u - \xi_s)(\sin\alpha - \cos\alpha \tan\delta) \tag{14}$$

To quantify the safety conditions, a factor of safety FS_ξ may be therefore defined as the ratio of the resistant and driving force:

$$\mathrm{FS}_\xi = \frac{T_f}{T} \tag{15}$$

The trend of the above factor of safety is ξ_s and is schematically represented in Fig. 10 for different values of the length of the unstable soil L_u and position of the resultant instabilising force. Note that in a design problem L_u can be interpreted as the longitudinal spacing of the reinforcement along the direction of the slope. It is easy to recognise that FS_ξ tends to infinity for ξ_s approaching H (as $q_{\lim}$ tends to infinity, Eq. 11) and for

Author's personal copy

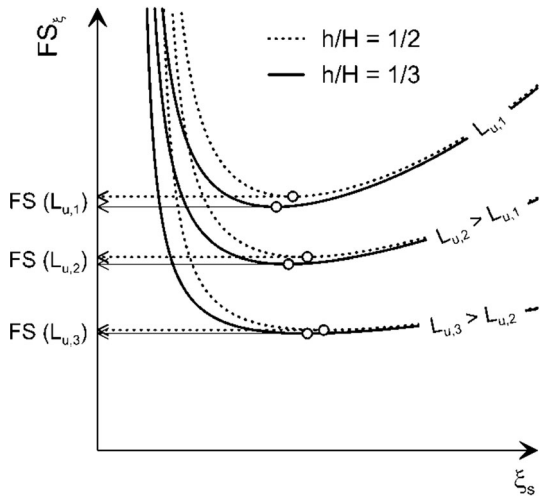

Fig. 10 Definition of factor of safety as function of L_u for different values of h/H

ξ_s approaching L_u (as the applied thrust T vanishes, Eq. 14) and therefore, for any L_u, there will exist a critical value of ξ_s corresponding to the minimum factor of safety. The latter thus represents the actual factor of safety FS for the specific set of L_u, H, h, α, δ, φ. By means of dimensional analysis, it would be simple to show that FS may be expressed as function of the five dimensionless parameters L_u/H, h/H, α/φ, δ/φ, φ. A simple spreadsheet can be therefore employed to explore the influence of such parameters on FS. Figure 11 depicts the factor of safety as function of L_u/H for different values assumed by the remaining problem parameters. Interestingly, FS is an increasing function of δ/φ, decreases with α/φ whereas is almost independent of the specific value assumed by the angle φ and the position assumed for the instabilising force. It is indeed evident from the graph that for $1/3 < h/H < 1/2$ and $25° < \varphi < 35°$ a very narrow range of FS is identified as function of L_u/H, α/φ and δ/φ, especially for the more realistic case of α/φ close to unity. The knowledge of the geometrical (α) and mechanical (δ and φ) properties of the unreinforced slope, combined with the selection of a required FS, leads to a value of L_u.

Recent design regulations like Eurocode 7 [6] employ a different approach, namely the Load and Resistance Factor Design (LRFD), where different partial factors are considered for driving forces and system resistance. In this logic, a mobilised shearing resistance angle ϕ_{mob}, lower than the actual one, is employed to calculate the conventional design capacity. Following the latter rationale, Fig. 12 reports the normalised reinforcement spacing L_u/H as function of α/ϕ_{mob} for different values of $\delta_{mob}/\varphi_{mob}$ (note that curves for different values of h/H and φ_{mob} are not distinguishable) and can be therefore directly utilised as a design chart.

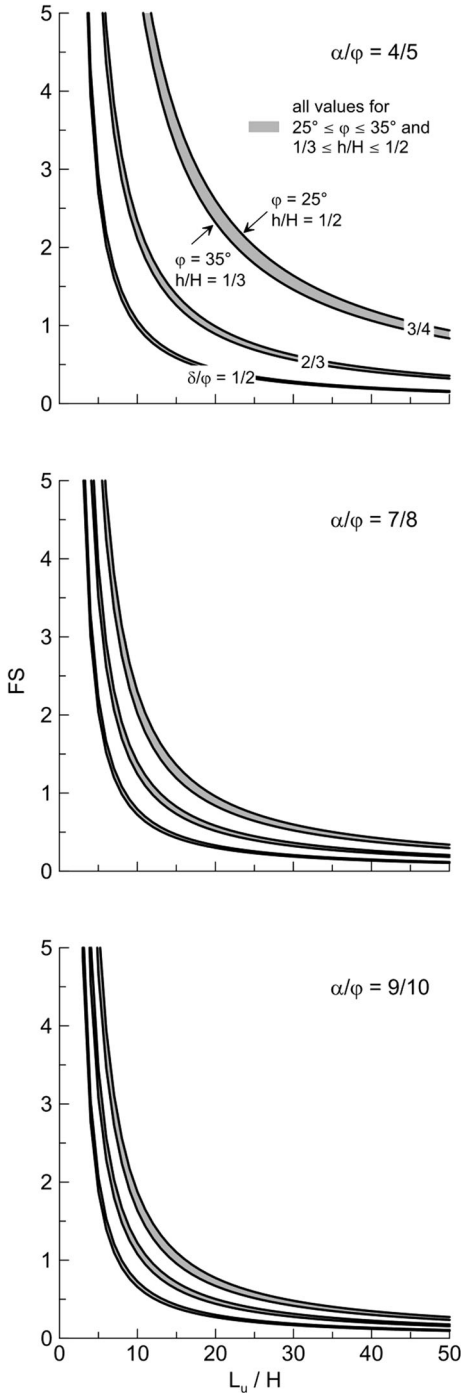

Fig. 11 Factor of safety as function of L_u/H, α/φ, δ/φ, h/H and φ

7 Conclusions

In this work, a novel method based on limit analysis is proposed to determine the spacing of closely spaced slope-stabilising piles or shafts. The method is based on the failure mechanism that a mass of unstable soil pushes a stable mass along a surface through the upper

Author's personal copy

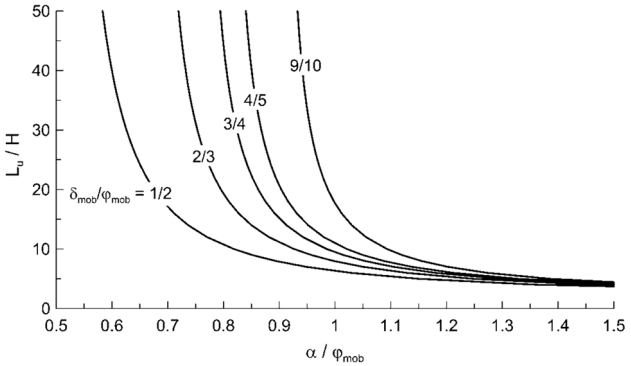

Fig. 12 Dimensionless spacing L_u/H as function of α/φ_{mob} and $\delta_{mob}/\varphi_{mob}$

end of the reinforcement. The main findings are summarised below:

1. The failure load for the stable mass is derived analytically and expressed in closed form by exploiting the upper bound theorem of the plastic collapse.
2. The analytical findings are validated by model tests in a geotechnical centrifuge. The comparison between the two approaches shows a remarkable predictive capability of the method.
3. A simple hyperbolic law, which implements small-strain soil stiffness and the failure load determined analytically, can be employed to reproduce the observed load–displacement curves at any point of the unreinforced slope.
4. The longitudinal spacing of the reinforcement elements is determined analytically. Design charts are provided following two different design approaches. Remarkably, the safety conditions of the slope practically depend only on three dimensionless parameters encompassing mechanical (α/φ, δ/φ) and geometrical (L_u/H) parameters, whereas they are almost insensitive to the friction angle φ and the position of the resultant force h/H.

It is fair to mention that real problems are often more complex than the idealised conditions analysed in the paper, which however represent necessary assumptions to obtain an analytical solution. Nevertheless, the design charts may be a help for the preliminary design.

Appendix

Derivation of Equation (4)

With reference to the triangle OCB (see Figs. 4 and 5), the law of sines assures that:

$$\frac{\sin \widehat{OCB}}{\overline{OB}} = \frac{\sin \widehat{COB}}{\overline{CB}} \tag{16}$$

By making use of the law of cosines:

$$\begin{aligned}\sin \Delta_2 &= \sin \widehat{OCB} \\ &= \sin \widehat{COB} \frac{\overline{OB}}{\sqrt{\overline{OB}^2 + \overline{OC}^2 - 2\overline{OB} \cdot \overline{OC} \cdot \cos \widehat{COB}}}\end{aligned} \tag{17}$$

and therefore:

$$\begin{aligned}\sin \Delta_2 &= \sin(\theta_s - \theta_0) \\ &\times \frac{r_0}{\sqrt{r_0^2 + r_0^2 e^{2(\theta_s-\theta_0)\tan\varphi} - 2r_0^2 e^{(\theta_s-\theta_0)\tan\varphi}\cos(\theta_s-\theta_0)}} \\ &= \sin(\theta_s - \theta_0) \\ &\times \left(1 + e^{2(\theta_s-\theta_0)\tan\varphi} - 2e^{(\theta_s-\theta_0)\tan\varphi}\cos(\theta_s-\theta_0)\right)^{-\frac{1}{2}}\end{aligned} \tag{18}$$

from which we obtain Eq. (4).

Derivation of Equation (11)

Solving Eq. (10) for $\dot{Q}$ and dividing both sides of the equation by $\dot{\omega}\gamma H^2(r_0\cos\varphi - h)$:

$$\begin{aligned}\frac{q_{\lim}}{\gamma H} = &\dot{\omega}\gamma\left[-\frac{1}{6}Hr_0(H\sin\alpha - 2r_0\cos\theta_0)\sin\varphi\right] \\ &+ \dot{\omega}\gamma\left[-\frac{1}{6}r_s\xi_s\left(\begin{matrix}2H\sin\alpha - 2r_0\cos\theta_0 \\ +\xi_s\cos\alpha\end{matrix}\right)\right. \\ &\left.\times\sin(\theta_s+\alpha)\right] \\ &(3\tan\varphi\cos\theta_s + \sin\theta_s)r_s^3 \\ &- \dot{\omega}\gamma\frac{-(3\tan\varphi\cos\theta_0 + \sin\theta_0)r_0^3}{3(1+9\tan^2\varphi)} \\ &+ \dot{\omega}\frac{c}{2\tan\varphi}\left(r_s^2 - r_0^2\right) \\ &\dot{\omega}\gamma H^2(r_0\cos\varphi - h)\end{aligned} \tag{19}$$

Multiplying both numerator and denominator of the right side of the above equation by $(6/H^3)$ one obtains Eq. (11).

References

1. Atkinson J (1993) An introduction to the mechanics of soils and foundations: through critical state soil mechanics. McGraw-Hill Book Company (UK) Ltd, New York
2. Ausilio E, Conte E, Dente G (2001) Stability analysis of slopes reinforced with piles. Comput Geotech 28(8):591–611

Author's personal copy

3. Baguelin F, Frank R, Said YH (1977) Theoretical study of lateral reaction mechanism of piles. Géotechnique 27(3):405–434
4. Baldi G, Belloni G, Maggioni W (1988) The ISMES geotechnical centrifuge. In: Corté JF (ed) Centrifuge 88, Paris. Balkema, Rotterdam, pp 45–48
5. Bosscher PJ, Gray DH (1986) Soil arching in sandy slopes. J Geotech Eng 112(6):626–645
6. CEN (2004). Eurocode 7 Geotechnical design. Part 1: General rules. European Committee for Standardization, Brussels
7. Chen WF (1975) Limit analysis and soil plasticity. Elsevier, Amsterdam
8. De Beer EE, Carpentier R (1977) Discussion of the paper by Ito and Matsui (1975). Soils Found 16(1):68–82
9. Drescher A, Detournay E (1993) Limit load in translational failure mechanisms for associative and non-associative materials. Géotechnique 43(3):443–456
10. Fioravante V (2000) Anisotropy of small strain stiffness of Ticino and Kenya sands from seismic wave propagation measured in triaxial testing. Soils Found 40(4):129–142
11. Fioravante V (2008) Physical modelling of landslide stabilization methods in an overconsolidated clay. Geotech Test J 31(2):175–191
12. Guo WD (2013) Simple model for nonlinear response of 52 laterally loaded piles. J Geotech Geoenviron Eng ASCE 139:234–252
13. Hassiotis S, Chameau JL, Gunaratne M (1997) Design method for stabilization of slopes with piles. J Geotech Geoenviron Eng ASCE 123(4):314–323
14. Hull TS (1993) Analysis of the stability of slopes with piles. In: Proceedings of the 12th Asian Geotechnical Conference, Singapore, pp 639–643
15. Ito T, Matsui T (1975) Methods to estimate lateral force acting on stabilizing piles. Soils Found 15(4):43–59
16. Kourkoulis R, Gelagoti F, Anastasopoulos I, Gazetas G (2011) Slope stabilizing piles and pile-groups: parametric study and design insights. J Geotech Geoenviron Eng ASCE 137(7):663–678
17. Kourkoulis R, Gelagoti F, Anastasopoulos I, Gazetas G (2012) Hybrid method for analysis and design of slope stabilizing piles. J Geotech Geoenviron Eng ASCE 138(1):1–14
18. Michalowski RL (1995) Slope stability analysis-a kinematical approach. Géotechnique 45(2):283–293
19. Muir Wood D (2004) Geotechnical modelling. Spon Press, New York
20. Muraro S, Madaschi A, Gaio A (2014) On the reliability of 3D numerical analyses on passive piles used for slope stabilisation in frictional soils. Géotechnique 64(6):486–492
21. Oakland MW, Chameau JLA (1984) Finite element analysis of drilled piers used for slope stabilization. In: Langer JA, Mosley ET, Thompson CD (eds) Laterally loaded deep foundations: analysis and performance, ASTM STP 835, pp 182–193. West Conshohocken, PA, USA: ASTM
22. Poulos HG (1995) Design of reinforcing piles to increase slope stability. Can Geotech J 32:808–818
23. Schofield AN (1980) Cambridge geotechnical centrifuge operations. Géotechnique 30(3):227–268
24. Viggiani C (1981) Ultimate lateral load on piles used to stabilize landslides. In: Proceedings of the 10th international conference on soil mechanics and foundation engineering, vol 3. Stockholm, Sweden, pp 555–560
25. Zhang G, Wang LP (2016) Integrated analysis of a coupled mechanism for the failure processes of pile-reinforced slopes. Acta Geotech 11:941–952
26. Zhang G, Wang LP, Wang YL (2017) Pile reinforcement mechanism of soil slopes. Acta Geotech 12:1035–1046